An Optical-Based Sensor for Automotive Exhaust Gas Temperature Measurement

Michal Prauzek, *Member, IEEE*, Radim Hercik, Jaromir Konecny, Martin Mikolajek, Martin Stankus, Jiri Koziorek, and Radek Martinek, *Senior Member, IEEE*

***Abstract*— The article introduces the design of an optical-based sensor that measures automotive exhaust gas temperatures (EGTs) over a wide temperature range. To measure temperature, we combined the luminescence method and the blackbody radiation (BBR) principle. We also developed our own measurement hardware that includes the means to process and evaluate the signals obtained for temperature conversion using optical methods for application in the target temperature range (−40 °C to 820 °C). This temperature range is specified by the automotive industry according to current combustion engine designs and emission requirements, which stipulate accurate measurement of operating temperature for optimal functioning. Current measurement solutions are based on the thermocouple principle. This approach is problematic, especially with regard to electromagnetic interference and self-diagnostics, and problems also exist with the gradual penetration of moisture into the temperature probe under extreme thermal stress. The case study confirmed the full functionality of the new optical sensor concept. The benefit of the proposed concept is full compatibility with existing conceptual solutions while maintaining the advantages of optical-based sensors. The results indicated that a combination of the BBR and luminescence methods with a ruby crystal in the proposed solution produced an average absolute error of 2.32 °C in the temperature range −40 °C to 820 °C over a measurement cycle time of 0.25 s.**

***Index Terms*— Automotive application, blackbody radiation (BBR), hybrid sensor, luminescence, optical-based sensor, optical fiber, optical signal analysis, temperature measurement.**

I. Introduction

THE automotive industry is an ever-growing area facing many research challenges. The number of vehicles operating on roads is increasing, and authorities are continually pushing harder for decreases in emissions [1].

Manuscript received 4 April 2022; revised 28 June 2022; accepted 6 July 2022. Date of publication 28 July 2022; date of current version 2 August 2022. This work was supported in part by the Project "Development of Algorithms and Systems for Control, Measurement and Safety Applications VIII" of the Student Grant System, VSB-TU Ostrava, under Project SP2022/11; in part by the European Regional Development Fund for the Research Centre of Advanced Mechatronic Systems Project through the Operational Program Research, Development and Education under Project CZ.02.1.01/0.0/0.0/16_019/0000867; and in part by the European Union's Horizon 2020 Research and Innovation Program under Grant 856670. The Associate Editor coordinating the review process was Dr. Jagadeesh Varadarajan Kumar. *(Corresponding author: Michal Prauzek.)*

The authors are with the Department of Cybernetics and Biomedical Engineering, VSB—Technical University of Ostrava, 708 00 Ostrava-Poruba, Czech Republic (e-mail: michal.prauzek@vsb.cz; radim.hercik@vsb.cz; jaromir.konecny@vsb.cz; martin.mikolajek@vsb.cz; martin.stankus@vsb.cz; jiri.koziorek@vsb.cz; radek.martinek@vsb.cz).

Digital Object Identifier 10.1109/TIM.2022.3192274

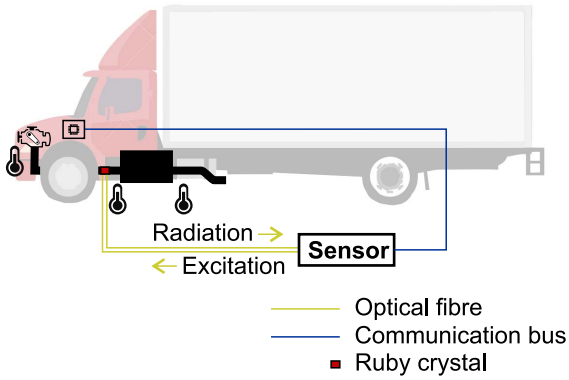

Fig. 1. Temperature sensor principle and application: targeted measurement points in vehicles, the principle of optical sensing (optical fibers), and communication with a central unit.

Although electric vehicles draw significant research interest [2], much research still targets the improvement of combustion engines [3] for more ecological operation. Optimal functionality in a combustion engine requires numerous sensors [4] that measure several properties of interest.

The aim of this study is to apply and examine an exhaust gas temperature (EGT) measurement method which is critical to optimal vehicle operation and effective emissions reduction [5]. Fig. 1 illustrates the principle and application of the temperature sensor described in this article. The proposed solution is designed for vehicles (cars, trucks, etc.) equipped with diesel combustion engines. Exhaust pipes have three locations where temperature must be measured: near the engine, in front of the diesel particulate filter (DPF), and behind the DPF.

Reliable and precise temperature measurement is a major challenge to the automotive industry. Combustion engines must be operated in a specific temperature range to achieve optimal operation, minimal emissions, and low fuel consumption. Thermocouples are commonly used in the automotive industry to measure temperatures, but their maximum measurable temperature, time response, accuracy, stability, and service life have limitations [6].

Optical-based thermometers are reliable, have an excellent measurable range, and are resistant to electromagnetic distortion [7].

Table I summarizes the state-of-the-art and advantages and disadvantages of current optical methods developed for

TABLE I
ADVANTAGES AND DISADVANTAGES OF CURRENT METHODS OF OPTICAL TEMPERATURE MEASUREMENT

Method	References	Advantages	Disadvantages
FBG	[8]–[12]	• Compact size • Resistant to chemicals • Immune to electromagnetic interference • Encapsulates structure provides durability • Widely applicable • Wide temperature range • Multiple sensors on a single optical fiber (one unit – multiple measurement points – grids)	• Complex processing unit • Problematic measurement of negative values • Complicated production of FBG (a separate, expensive phase mask must be prepared for each grid with a different Bragg wavelength) • Problematic compliance with automotive requirements, low signal level • Measurement speed depends on the thermal conductivity of the sensor housing and the surface of the measured object. • Mechanical deformation (e.g., shock) causes measurement uncertainty
BBR	[8], [13]–[17]	• Contactless, ability to measure at greater distances, quick response and negligible effect from a measured object • Linearity of measurements across a wide range of temperatures and easy evaluation • Simple production principle, simple processing electronics	• Error caused by an uncertainty in determining the emissivity of a measured body • Error caused by environmental permeability • Error caused by radiation reflected from the surroundings; temperature cannot be measured below the sensor's own temperature
Luminescence	[18]–[28]	• Measurement of low and sub-zero temperatures	• Longer time required to process data, problematic calibration • Time instabilities, low signal level • Ambient temperature fluctuations affect the output signal • Reference signal required • Relatively small range of measured temperature (only a few hundred °C)
Hybrid (our solution)		• Suitable for automotive purposes – wide temperature range (positive and sub-zero temperatures) • Widely applicable • Two-wire connection • Quick response • High accuracy in working areas defined according to automotive requirements • Able to measure very quick temperature changes	• High inaccuracy at certain temperature intervals • Complex evaluation algorithm • More complex calibration

temperature measurement. Optical thermometers employ several physical principles, for example, blackbody radiation (BBR) [13], which is based on Plank's law and used in high-temperature measurement [8]. The BBR method has applications in fields such as aerospace [15], medicine [17], and manufacturing [14].

Luminescence fiber-optic temperature sensors based on the principle of measuring luminous intensity can be used as an alternative temperature measurement method. In this case, a pulse excitation light is emitted by a light source into fluorescent material and the subsequently emitted fluorescent signal is transmitted to a photoelectric detector. The fluorescent signal is then converted into electrical signals, and temperature is calculated according to the time response or detected amplitude [27]. The temperature sensor's range is significantly dependent on the luminescence material [18], [20], [21]. Zhang *et al.* [19] provide an overview of the state-of-the-art co-doped materials used for purposes based on luminescence principles. High-temperature optical probes that apply the luminescence principle have also been constructed and proved effective [28].

Advances from research in laser technology and fiber Bragg grating (FBG) sensors now allow greater possibilities in the development of optical thermometers. The principle involves the transmission of broadband light into an FBG, where a light wave that conforms with the Bragg condition is reflected to generate a reflection spectrum. A change in a sapphire fiber grating temperature results in a variation in the effective refractive index, and therefore the reflected light's wavelength will change. The reflected light is captured by a spectral analyzer, and the temperature is obtained through demodulation of the reflected spectrum [8]. FBGs are also cross-sensitive to strains [29]. A strain caused by a mismatch in thermal expansion of the fiber grating material and the host specimen leads to an extra shift in the Bragg wavelength in the FBG [30]. The cross-sensitivity between temperature and strain in the sapphire FBG must therefore be evaluated accurately [31]. Resen *et al.* [9] proposed a new, efficient optical heterodyne interrogation system for optical sensors. FBG can also be used to monitor various parameters, such as soil moisture [12] or air humidity [10].

The presented solution introduces a new type of automotive sensor that combines the luminescence method from a ruby crystal and BBR to replace the widely used thermocouple sensor type [32], which has many disadvantages and is especially susceptible to electromagnetic noise. Optical sensors

solve these disadvantages, but manufacturing and total costs are principally higher than thermocouple solutions. The aim of developing a new sensor is to find an optimal tradeoff between higher cost and superior properties. The article contributes with the novel use of two optical principles to develop a cost-effective sensor that is resistant to electromagnetic interference, possesses self-diagnostic abilities, and is immune to the gradual penetration of moisture into the temperature probe under extreme thermal stress. With respect to automotive requirements, the final cost should be as low as possible. FBGs provide sufficient technical parameters; however, the cost of a processing unit is relatively high due to the requirements for signal acquisition, data processing, and spectral analysis. Sapphire fiber also has an excellent temperature range (up to 2000 °C). Sapphire fiber significantly increases product price, however [8]. We, therefore, employed a low-cost glass optical fiber with a simple photodiode as a photodetector.

The article contains six sections. Section I provides a general description of the target and application area and a brief overview of the state-of-the-art. Section II details the sensor's design, including automotive requirements, probe construction, electronic design, measurement cycle, and temperature calculation. Section III describes the virtual instrumentation measurement system and experimental setup. Section IV presents the final results. Section V contains a discussion, and Section VI concludes the article with outlines for future work.

II. Sensor Design

High-temperature sensors in the automotive industry are mainly used to measure temperatures in the exhaust subsystem, especially in front of and behind the DPF. Measurement is performed directly in the exhaust path from the engine to ensure optimal engine operation with safe operating conditions and low emissions [33].

Thermocouples consist of two metal wires made of different materials/alloys connected at one end. The most important aspect to consider in selecting two suitable materials is the thermoelectric difference that exists between them. The automotive industry uses K-type and N-type thermocouples. The N-type is a newer alternative to the K-type, permitting higher temperatures and being more resistant to oxidation [34]. The N-type thermocouple allows the measurement of temperatures in the range −270 °C to 1300 °C. The aim of developing an optical sensor is to satisfy the target temperature measurement range accuracy in accordance with the requirements of the application area. The main benefit of an optical sensor solution is resistance to electromagnetic interference and moisture.

A. Automotive Requirements

The proposed temperature sensor has four zones with different thermal load requirements (see Fig. 2). Zone A is exposed to temperatures of −40 °C to 800 °C and located directly in the exhaust pipe. Zone B is where the temperature probe is firmly attached to the flue gas path and must withstand temperatures of −40 °C to 300 °C. Zone C is the cable that connects the probe to the sensor's evaluation electronics and is exposed to temperatures of −40 °C to 200 °C. Zone D contains the sensor's electronics and must withstand temperatures of −40 °C to 155 °C.

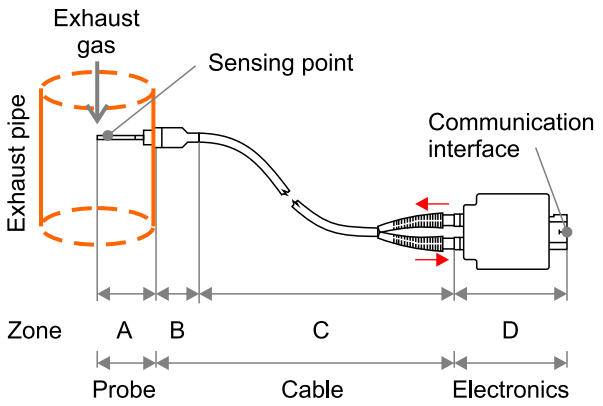

Fig. 2. Detailed composition of the temperature sensor (probe, cable, and electronics used for analysis). The zones are divided according to temperature resistance requirements.

TABLE II
Required Accuracy for Sensor Temperature Ranges

Temperature	Maximum error
−40°C to 20°C	±5°C
20°C to 150°C	±10°C
150°C to 820°C	±5°C

Table II shows the target accuracy of the final sensor solution. The usual working range of the EGT probe is 150 °C–820 °C and requires a high measurement accuracy of ±5 °C. The low-temperature range of −40 °C to 20 °C is important during engine cold starts and also requires high accuracy [35]. Measurement accuracy in the range 20 °C–150 °C is not critical, mainly because hot flue gases which fall into this temperature range pass through the exhaust system quickly and are present only for several seconds [36].

Measurement accuracy according to these requirements must be guaranteed for the lifetime of the EGT sensor, although 1000 h of operation is considered a minimum in the automotive industry. This figure corresponds to the planned service life of the vehicle. Since the complete solution should be cost-effective, we selected glass fiber as a suitable component.

B. Probe Construction

The sensing component is depicted in Fig. 3 and consists of a stainless steel tube that contains a pair of optical fibers touching the ruby crystal. The optical fibers have a diameter of 660 μm. Instead of a heat-resistant polyamide, the fiber is protected by a ceramic insert which simultaneously affixes the ruby crystal and fibers into place.

The ruby crystal is the core of the sensing element. It is cylindrical in shape with a length of 2.5 mm and a diameter of 1.8 mm. The optical fibers are placed on one side of the crystal, which is polished to increase optical transmission. The other side of the temperature probe consists of a terminal with a metric thread, which contains the special optical connector

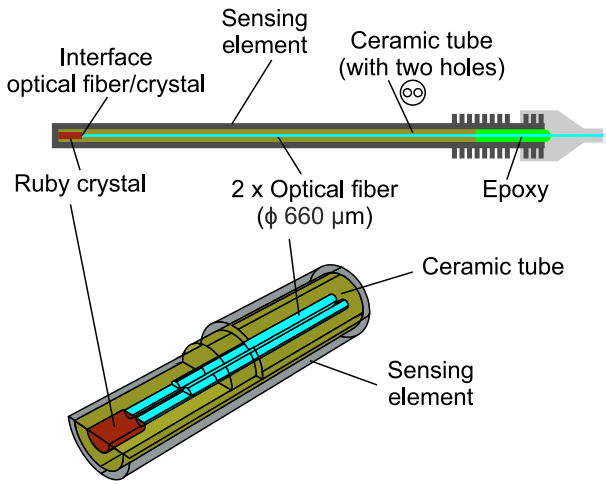

Fig. 3. Design of the sensing element in the probe and detail of the hot end (ruby crystal, optical fibers, and ceramic tube with two holes).

TABLE III
THERMAL EXPANSION COEFFICIENTS OF THE MATERIALS USED IN THE SENSOR

Material	Thermal expansion (μm/K)
Ceramic tube	7.3
Ruby crystal	6.2
Silicon optical fiber	5.0
Stainless steel	16.5

for connecting the optical cable. The probe assembly is sealed with a high-temperature epoxy sealant.

The probe's design maintains a tight seal which minimizes the effect of vibrations (see detail in Fig. 3). Direct contact is provided by the polished end of the optical fiber and crystal. If an expansion gap occurs because of vibrations or thermal expansion, the optical signal should still be able to pass through the expansion gap without significantly affecting the output signal's quality. This is mainly because the size of the expansion gap is insignificant, and the polished surfaces of the optical fibers and a crystal are fixed in the ceramic tube and remain perpendicular.

Thermal expansion was reduced by using the selected materials. The ruby crystal, which is the core of the probe, is inserted into a ceramic tube containing two drilled holes for the silicon optical fibers. A high-temperature sealant is applied at the cooler end of the probe. The main feature these materials have in common is similar coefficients of thermal expansion (CTE) (see Table III), thereby minimizing any changes in coupling efficiency. The only material which has a greater CTE is the stainless-steel probe shroud. However, thermal expansion in the shroud not only occurs along its length but also its volume, resulting in an internal pressure that stabilizes the crystal, ceramic filling, and optical fibers.

An expansion gap reduces the coupling efficiency between the light signal and the optical fiber. Testing showed that the excitation light and luminescence light power reduced significantly as the temperature increased, indicating a decrease in the optical coupling efficiency. This is confirmed in the spectrum given in Fig. 5. The thermal expansion effect represents the time-invariant for a given temperature and could therefore be compensated for with calibration. Calibration could also compensate for the manufacturing tolerances which occur during the production of the crystal-fiber coupling.

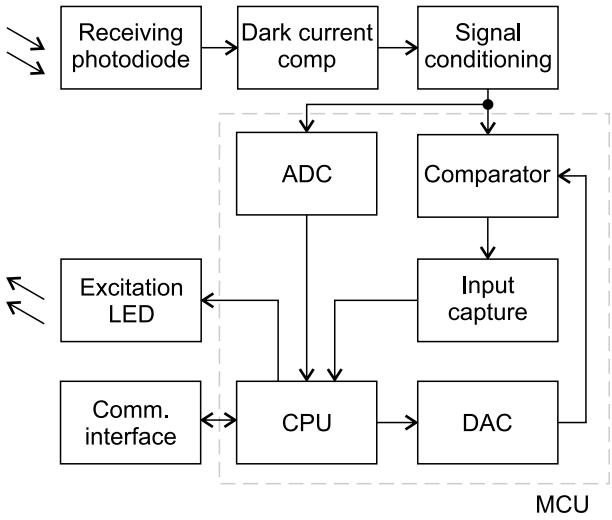

Fig. 4. Simplified block diagram of the electronics: MCU with peripherals, communications interface, the excitation LED, and analog front-end with receiving photodiode.

C. Sensor Evaluation Electronics

This section describes the sensor electronics evaluation unit. Fig. 4 presents a simplified block diagram of the unit. The sensor electronics contain an excitation light-emitting diode (LED) and receiving photodiode. The LED is driven by a microcontroller unit (MCU) and is used to excite the luminescent effect of the ruby crystal. The receiving photodiode measures the optical response of the ruby crystal, and the resulting output from the photodiode is delivered to a dark current compensator and signal processing circuit. The signal is then processed by the MCU, which uses an analog comparator and input capture circuit. A 16-b analog-to-digital converter (ADC) block is then used to measure the BBR signal and amplitudes during low temperatures.

Dark current compensation is based on measuring the receiving photodiode transition temperature from the voltage drop which occurs across the photodiode by using the circuit for monitoring the reference voltage and connecting the anode and cathode voltages of the photocell to a cathode with a reference voltage via a calibration resistor. The amount of compensation can then be calibrated by the magnitude of the resistance of the calibration resistor. Its size depends on the internal resistance of the photodiode.

Accurate measurement of luminescence time is ensured by using a comparator, which defines the threshold amplitude of the signal at the end of the limitation effect, in combination with an input capture circuit and subsequent use of a direct memory access module.

An LED with a nominal 465-nm wavelength is used as an excitation source. Luminescence is produced in the ruby crystal, and the excited light is emitted at a wavelength of

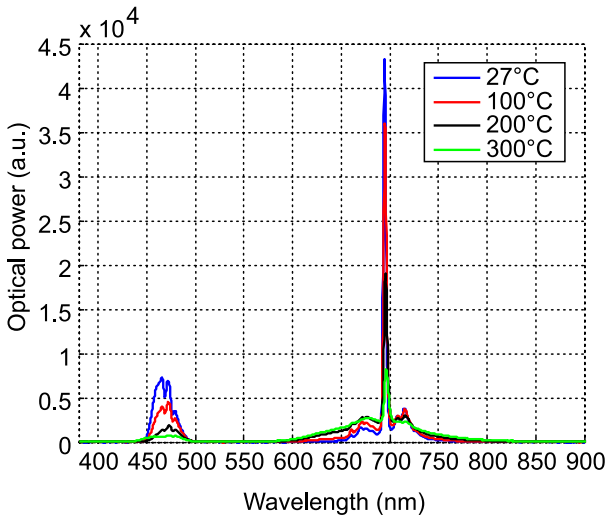

Fig. 5. Optical power spectrum of the ruby crystal excited at $\lambda = 465$ nm.

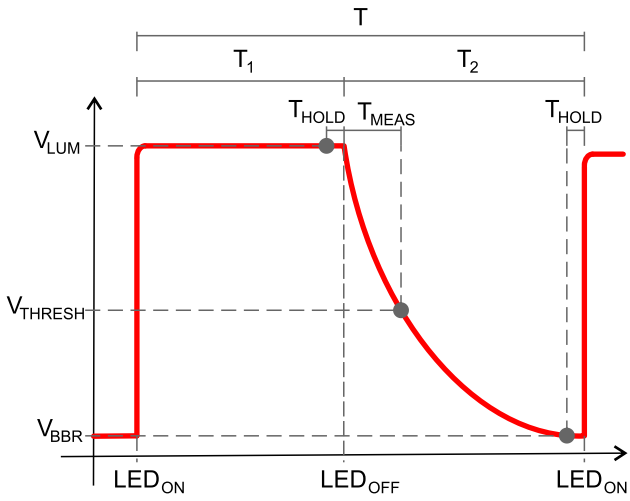

Fig. 6. Single measurement cycle: Luminescence (V_{LUM})—BBR (V_{BBR}), voltage level measurement, and time measurement (T_{MEAS}).

around 695 nm (see Fig. 5). A photodiode with high sensitivity at 695 nm is therefore positioned on the receiving side. A polarizing filter is also inserted between the photodiode and fiber to eliminate any interfering wavelengths.

D. Measurement Cycle

To compute the temperature value, two voltages and a single time value are measured. The measurements must be synchronized with the excitation light source cycle, as depicted in Fig. 6.

The waveform denotes the LED state. The LED is switched ON and OFF during each measurement cycle; respective times are denoted T_1 (the LED is ON) and T_2 (the LED is OFF). Before any change in the LED's state, the voltage adjusted by the signal conditioning block (see Fig. 4) is measured using the MCU's built-in ADC. Measurements are taken only after the voltage value has settled. This is accomplished by starting the respective ADC measurement in advance

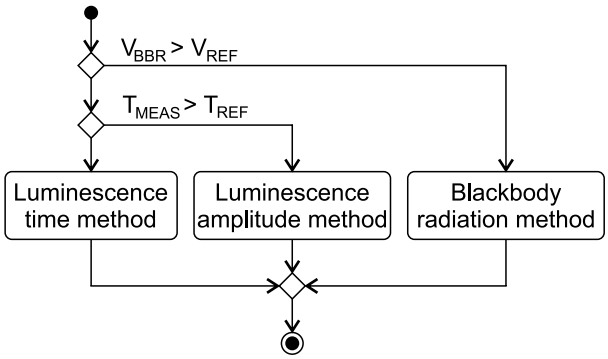

Fig. 7. Principle of switching between luminescence time, luminescence amplitude, and BBR methods.

immediately before the LED changes state. During this time, denoted T_{HOLD}, the voltage should be constant. Two voltage values are acquired in each measurement cycle: V_{LUM} of the luminescence phase and V_{BBR} of the blackbody phase.

The V_{LUM} value is used to compute V_{THRESH} according to the following equation:

$$V_{\mathrm{THRESH}} = V_{\mathrm{LUM}} - V_{\mathrm{DIFF}} \ (\mathrm{V}) \tag{1}$$

where V_{DIFF} is a fixed parameter that affects the possible temperature range, which can be estimated using the luminescence time method and maximal T_{MEAS}.

In the next step, T_{MEAS} is measured. The obtained V_{THRESH} value is switched to the output of the digital-to-analog converter (DAC). As depicted by Fig. 6, the MCU has an integrated analog comparator. The comparator's noninverting input is connected to the voltage generated by the signal conditioning block. The inverting input is connected to V_{THRESH}. The output signal of the comparator is therefore asserted whenever the input voltage is less than V_{THRESH}. The output of the comparator is used to trigger the input capture module. The input capture module integrates a 32-b timer with a 1-MHz clock input; the timer is activated when the LED is switched off ($\mathrm{LED}_{\mathrm{off}}$ event) and stopped when the comparator output is asserted.

E. Temperature Calculation

When the sensor has measured all parameters in one cycle (V_{BBR}, V_{LUM}, T_{MEAS}), the current temperature is calculated. The sensor uses two optical methods (BBR and luminescence), although three principles are applied to estimate temperature. Using the BBR method, the sensor calculates temperature based on the amplitude outside excitation. Using the luminescence method, the sensor switches between estimations derived from measured time and amplitude.

Fig. 7 illustrates the principle of switching methods. First, the evaluation algorithm checks whether a sufficient level (V_{REF}) of BBR exists outside the excitation phase. If true, the probe temperature is calculated using the V_{BBR} parameter. When the V_{BBR} parameter does not reach a sufficient level, the luminescence method is used. If T_{MEAS} is less than reference T_{REF}, the algorithm calculates according to the time method;

in the other case, the temperature is calculated using the amplitude method.

Each method applies the same principle to estimate probe temperature [37]. Evaluation is based on a quartic function [see (2)], where parameter p represents the measured value V_{BBR}, V_{LUM} or T_{MEAS} according to the method used

$$\mathrm{TEMP} = ap^4 + bp^3 + cp^2 + dp + e. \tag{2}$$

Each method (BBR, luminescence time, and luminescence amplitude) has an individual set of parameters (a, b, c, d, and e). This set was estimated from the experimental measurement performed during sensor prototyping. This set of parameters is also stored in the nonvolatile memory contained in the sensor's electronics and therefore updated during calibration. For this reason, each sensor has three unique sets of calibration values.

III. Experimental Instrumentation

This section describes the virtual instrumentation and setup for measuring and evaluating temperatures and a description of the experiment's procedure.

A. Virtual Instrumentation Measurement System

Accurate and reliable testing in the target EGT range is an important part of the proposed sensor. For the purposes of the case study, we designed a modular measurement system based on virtual instrumentation. The aim of the design was its ability to objectively verify the full functionality, accuracy, and stability of the proposed optical sensor with the relevant reference according to scenarios defined by automotive industry specifications (temperature range, humidity, dynamic temperature changes, etc.). Testing was performed under precisely defined laboratory conditions using a commercially available calibrated thermocouple (K-type) as reference. Hardware components (NI-9223) implemented with the CompactDAQ platform were used for data collection, processing, and analysis. Fig. 8 depicts a simplified scheme of the experimental workplace. The measurement system consisted of three blocks: 1) optical sensor; 2) reference thermocouple; and 3) virtual instrumentation measurement system.

The virtual instrument measurement system shown in Fig. 8 executes a collection procedure for analog signals from the tested sensor located in the experimental furnace. Measurement is performed with two NI-9223 measuring cards, which have a four-channel simultaneous input (±10 V, 1 M/s, 16-bit). Synchronization is provided by cDAQ-9158, which is connected to the measuring computer via Ethernet. The virtual sensor obtains data in parallel from the two UART channels of the electronics.

B. Experimental Procedure

The aim of the experimental procedure was to test the sensors in the EGT measurement range (−40 °C to 820 °C). The testing procedure was divided into two stages because of the different requirements for cooling and heating (see Table IV).

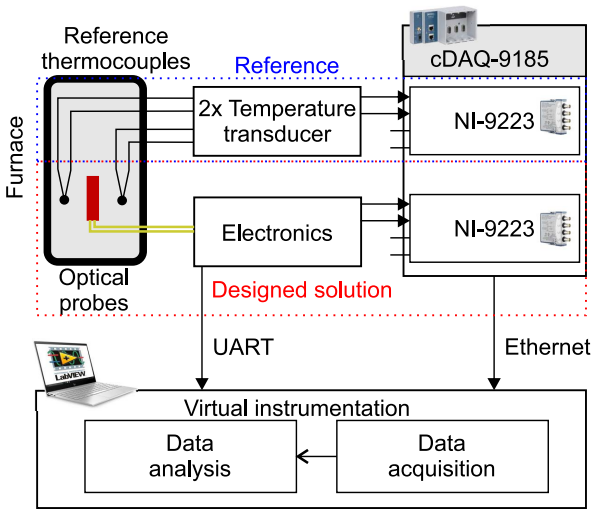

Fig. 8. Instrumentation diagram: measurement using an optical probe, electronics, a reference thermocouple with NI modules, and the LabView application on a PC.

TABLE IV
Heating and Cooling Process

Process	Start temperature	Stop temperature
Cooling	−45 °C	20 °C
Heating	830 °C	25 °C

Cooling was achieved with liquid nitrogen placed inside the furnace to cool the internal space to −45 °C. The furnace was then heated by ambient temperature to 20 °C. The second stage was the heating process. Generally, the BBR method can be used without any temperature limits. In the presented solution, we used glass optical fibers with a softening point of 846 °C and a melting point of 1121 °C. The maximum temperature was therefore set to 830 °C to avoid any mechanical problems. To reduce significant electrical noise from heating elements, the furnace was tempered to 830 °C. When target the temperature was reached, the cooling process began and the furnace was allowed to cool to a temperature of approximately 25 °C over 12 h. The process of slowly cooling the furnace minimized rapid temperature differences in the space between the probe and the reference thermocouple. A slower cooling process also allowed sufficient time to capture signals during stable temperatures. The experimental procedure was repeated four times on one sensor prototype.

IV. Results

This section contains two parts: the first part shows the dependence of the measured parameters on various temperatures through a time-domain analysis of one of the tested sensors; the second part includes an analysis of the total absolute error of the sensor prototype in the EGT measurement range.

A. Results of the Time-Domain Analysis

Temperature estimation is dependent on the character of the measured signal. The character of the received photodiode signal at various temperatures is described below.

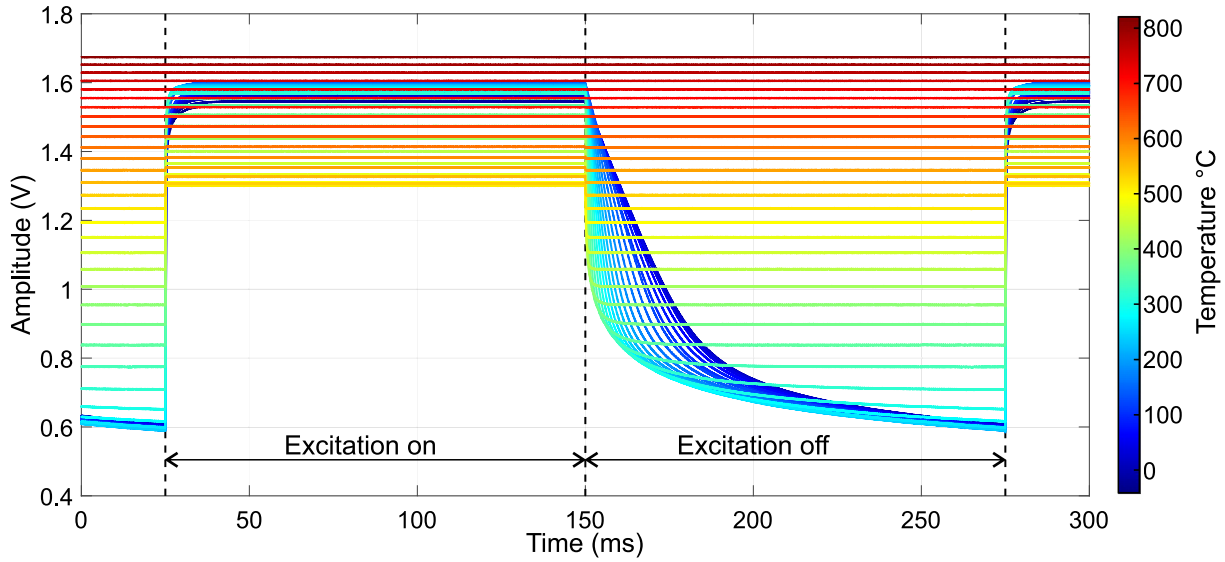

Fig. 9. Measured voltage signals at the analog front-end (receiving photodiode) in the range −40 °C to 820 °C.

TABLE V
OVERVIEW OF MEASURED PARAMETERS IN THE RANGE −40 °C TO 820 °C

Temperature (°C)	V_{LUM} (V)	V_{BBR} (V)	V_{TRESH} (V)	T_{MEAS} (ms)	Temperature (°C)	V_{LUM} (V)	V_{BBR} (V)	V_{TRESH} (V)	T_{MEAS} (ms)
−40	1.536	0.601	1.336	7.759	400	1.475	0.940	1.275	0.367
−20	1.546	0.601	1.346	7.859	420	1.447	1.004	1.247	0.233
0	1.557	0.600	1.357	7.792	440	1.410	1.054	1.210	0.233
20	1.564	0.598	1.364	7.692	460	1.374	1.104	1.174	0.233
40	1.570	0.598	1.370	7.493	480	1.334	1.146	1.134	NA
60	1.573	0.597	1.373	7.059	500	1.313	1.183	1.113	NA
80	1.575	0.592	1.375	6.593	520	1.304	1.231	1.104	NA
100	1.577	0.592	1.377	6.06	540	1.310	1.263	1.110	NA
120	1.600	0.590	1.400	5.595	560	1.330	1.308	1.130	NA
140	1.600	0.589	1.400	4.961	580	1.356	1.343	1.156	NA
160	1.597	0.588	1.397	4.329	600	1.386	1.371	1.186	NA
180	1.596	0.585	1.396	3.73	620	1.416	1.403	1.216	NA
200	1.594	0.584	1.394	3.263	640	1.447	1.437	1.247	NA
220	1.593	0.587	1.393	2.798	660	1.475	1.466	1.275	NA
240	1.591	0.585	1.391	2.398	680	1.503	1.499	1.303	NA
260	1.588	0.595	1.388	2.097	700	1.530	1.522	1.330	NA
280	1.584	0.609	1.384	1.798	720	1.557	1.550	1.357	NA
300	1.579	0.649	1.379	1.465	740	1.582	1.575	1.382	NA
320	1.570	0.701	1.370	1.232	760	1.607	1.599	1.407	NA
340	1.556	0.763	1.356	0.966	780	1.630	1.628	1.430	NA
360	1.539	0.835	1.339	0.699	800	1.653	1.647	1.453	NA
380	1.508	0.893	1.308	0.533	820	1.675	1.669	1.475	NA

Fig. 9 charts the receiving photodiode voltages for temperatures in the range −40 °C to 820 °C, and Table V provides a numerical overview of the measured parameters.

The measurement period (T) in the experiment was set to 250 ms and divided into two excitation phase intervals (T_1, T_2), each with a duration of 125 ms. In future experiments, the excitation phase intervals can be optimized. T_2 is directly dependent on the luminescence of the ruby crystal. This time can be decreased only with the use of a ruby crystal with a different chrome concentration. Excitation time is dependent on several physical aspects: the first stage of excitation is absorption by the ruby crystal, lasting approximately 50 ms; for the remaining time (75 ms), the amplitude is sampled. The total measurement time has another option for optimization. When the BBR method is used for high-temperature situations (>350 °C), excitation can be switched off until V_{BBR} becomes insufficient. In this case, the sensor's response time is limited only by the ADC's sample frequency.

Temperature values can be estimated according to three methods, as described in Section II-E. If V_{BBR} is less than the voltage reference ($V_{\mathrm{REF}} = 0.65$ V), the temperature is less than 350 °C and the luminescence method is used. For the lower temperature range of −40 °C to 60 °C, the temperature is calculated from the excitation amplitude level (V_{LUM}) since excitation time is not dependent on temperature. For the temperature range of 60 °C–350 °C, excitation time is used to obtain temperatures since the excitation time (T_{MEAS}) changes more significantly than V_{LUM}.

TABLE VI

EFFECT OF V_{DIFF} VALUES ON THE ABILITY TO MEASURE USING THE LUMINESCENCE TIME METHOD

V_{DIFF} (V)	T_{MAX} (°C)	t_{MAX} (ms)
0.05	520	1.5
0.10	500	3.5
0.15	480	3.7
0.2	**460**	**7.8**
0.3	440	12.2
0.4	420	16.6
0.6	380	26.9
0.8	320	49.8

When the temperature exceeds 350 °C, V_{BBR} is greater than the voltage reference, and BBR is used (i.e., the temperature is evaluated from V_{BBR}). It is interesting that V_{BBR} rises, whereas V_{LUM} falls (approx. temperature range of 350 °C–520 °C). This phenomenon results from a part of a ruby crystal luminescence power spectrum being shifted to shorter wavelengths by higher temperatures occurring beyond the photodetector's area of sensitivity. Therefore, the detector in the electronics of the sensor can capture only a portion of the emitted luminescence light, resulting in a lower voltage at the amplifier's output. From a temperature of 420 °C, the excitation time T_{MEAS} is constant, but from 480 °C, it is not possible to measure T_{MEAS} cannot because of saturation caused by BBR.

Table VI shows the results of a case study for various V_{DIFF} settings. The value of V_{DIFF} affects the maximum measurable temperature. A lower V_{DIFF} permits the measurement of higher temperatures using the time luminescence method, but the time range rapidly diminishes. The proposed solution used $V_{DIFF} = 0.2$ V. A lower V_{DIFF} increases the temperature range by 20 °C, but t_{MAX}, which reflects the accuracy of the time luminescence method, decreases by more than 50%. A higher V_{DIFF} decreases the temperature range, and it is unnecessary to obtain a longer t_{MAX}, 7.8 ms being sufficient to accurately measure falling time.

The parameter V_{REF} must take into account the principle of BBR. This V_{REF} value should be greater than the BBR noise caused by ambient temperature and the temperature of the optical cable. V_{REF} must also be less than V_{LUM}, in our case falling in the range 0.7–1 V. The parameter T_{REF} must take into account the physical principle of luminescence. When the temperature is low, the value T_{MEAS} does not sufficiently change. The proposed solution used $T_{REF} = 7$ ms.

B. Absolute Error of the Sensor Prototype

The proposed solution was tested on a sensor prototype. The total absolute error was calculated as an extended uncertainty for $k = 3$ (99.7% centile) and represented 2.32 °C. In terms of EGT measurement, the most significant temperature ranges are during engine cold start (−40 °C to 20 °C) and when exhaust gases reach temperatures greater than 600 °C. The temperature range 20 °C–150 °C is not critical to proper engine functionality since exhaust gases reach this temperature range only during the first few seconds of engine operation.

Table VII shows the total absolute errors in the specified ranges for the sensor prototype. A comparison of the total absolute temperature errors with the ranges specified in the automotive requirements section (see Table II) indicates that the sensor fulfilled the specified requirements.

TABLE VII

ERRORS IN THE TEMPERATURE INTERVALS FOR THE SENSOR PROTOTYPE ACCORDING TO THE AUTOMOTIVE REQUIREMENTS AND FOUR MEASUREMENTS

Range (°C)	Average absolute error (°C)	Requirements (°C)
−40 to 20	1.97	±5
20 to 150	4.44	±10
150 to 820	1.61	±5

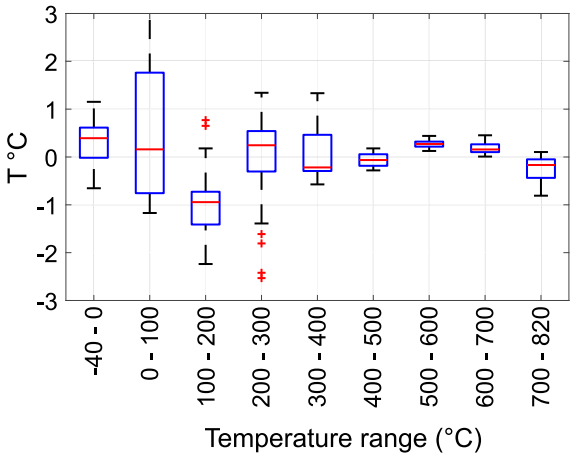

Fig. 10. Summary boxplots of absolute errors in the sensor prototype in the range −40 °C to 820 °C for four measurements.

TABLE VIII

SUMMARY OF ABSOLUTE ERRORS IN THE SENSOR PROTOTYPE FOR THE SPECIFIED TEMPERATURE RANGES AND FOUR MEASUREMENTS

Range (°C)	Average absolute error (°C)
−40–0	1.57
0–100	4.27
100–200	1.72
200–300	2.29
300–400	1.52
400–500	0.40
500–600	0.23
600–700	0.33
700–820	0.73

Fig. 10 plots the absolute errors in the sensor prototype for the range −40 °C to 820 °C.

The experiments confirmed the hypotheses of using a hybrid optical sensor for EGT measurements. The results presented in Table VIII and Fig. 10 show the absolute errors for specific temperature ranges. The main problem with currently available optical sensors is the measurement of negative temperatures in the range −40 °C to 0 °C, where the proposed solution produced an absolute error of less than 2 °C: this fully reflects the automotive requirements for EGT measurement. Positive values were analyzed in 100 °C intervals, and according to engine specifications, the working temperature of a fully loaded and unloaded combustion engine is from 400 °C to 700 °C. Our solution achieved an accuracy within 0.5 °C in this range. High accuracy in this area is the most critical aspect of the target application. The absolute error was less than 2 °C in the range 100 °C–400 °C, and the largest measurement error was in the range 0 °C–100 °C.

TABLE IX
COMPARISON WITH STATE-OF-THE-ART OPTICAL SENSORS

Ref.	Range	Result properties
[38]	25–200 °C	resolution 0.13 °C
[28]	20–600 °C	luminescence lifetime analysis
[27]	0–90 °C	max. error 0.45 °C
[39]	200–1,000 °C	resolution 0.45 °C, hysteresis ±4 °C
Hybrid (our solution)	−40–820 °C	absolute error 2.32 °C

V. DISCUSSION

The aim of the work was to develop a replacement for an existing EGT sensor solution which is based on the thermocouple principle. From a design point of view, the replacement solution is innovative and delivers several advantages. The thermocouple measuring principle was replaced with an optical-based temperature measurement method using a ruby crystal and two optical fibers in combination with evaluation electronics. The sensor applies the luminescent and BBR measurement principles. The external mechanical dimensions of the sensor are compatible with the existing solution, and no further modifications are required in vehicle construction.

Based on our mechanical resistance tests, the newly developed sensor demonstrates similar mechanical properties. The service life of the sensing component of the sensor is 1000 h. Beyond this time, exposure to high temperatures begins to degrade the optical fiber cores and measurement accuracy reduces. The undisputed advantage of the solution is the absolute resistance of the sensing component and the sensor's optical cable to EMC and EMI. It is therefore possible to place the sensor's sensing component near very strong sources of electromagnetic radiation.

The sensor's main feature is its measurement accuracy specified by the requirements of the automotive industry. Our analysis and evaluation of long-term measurements indicate that the proposed sensor meets the accuracy requirements across the entire range. The absolute error varies within the entire range, a result obtained by using three different measurement methods. The BBR method attains the highest accuracy since the light is emitted directly by a ruby crystal and fiber. The luminescence method produces higher absolute error values as a result of excitation requirements.

The proposed solution has a wide measurement range, and therefore the properties of the results are discussed in parts. Table IX compares the accuracy with other optical sensor solutions. Wang *et al.* [38] declared a measurement resolution of 0.13 °C. The resolution of our solution varies with the measurement method applied. With the amplitude method (low temperatures and BBR), the resolution is determined by a 16-b ADC. The resolutions for the proposed solution at low temperatures are 0.136 °C and 0.026 °C using the BBR method. Resolution for the time-based luminescence method is derived from the input capture module's 1-MHz clock signal; the resulting resolution for the time-based method is 0.039 °C.

Jinling and Junhai [28] stated that the luminescence time method was not suitable for negative temperature measurement, which we also confirm in our study, where the amplitude-based approach is used in the temperature range −40 °C to 65 °C. The study in [28] used the time-based method up to 600 °C, but in our solution, the measurement range is extended to 820 °C by using the BBR method.

Zhao *et al.* [27] presented a low-temperature range sensor (0 °C–90 °C) with a maximum error of 0.45 °C using the time-based method. Our solution combines two methods within this range, resulting in a higher absolute error of 4.27 °C, although the absolute error still satisfies automotive requirements since engine operating temperatures fall outside this range.

The study [39] declared a temperature range of 200 °C to 1000 °C, with a resolution of 0.45 °C and hysteresis of ±4 °C. Hysteresis relates to the absolute error, as the difference between the measured value and the true value might differ according to the hysteresis of ±4 °C. We did not analyze hysteresis in our solution, although we used the BBR method in the high-temperature range, and therefore the resolution is approximately ten times higher, resulting mainly from using a different approach to estimating temperature.

VI. CONCLUSION

The presented case study clearly demonstrated the optical sensor's full functionality for application in an EGT measurement range. The solution satisfies automotive industry standards, and the sensor design is fully compatible with currently used sensors in dimensions, encapsulation, power requirements, and so on. The experiments applied drop-down tests starting from a high temperature to analyze the sensor across a broad temperature range. For this reason, we did not evaluate the hysteresis of the proposed sensor.

The combination of luminescence and BBR principles covers the operating temperature spectrum of the required application and therefore provides high accuracy across the operating temperature range. The proposed solution fully reflects the advantages of optical-based sensors, which includes resistance to electromagnetic interference, environmental friendliness, and small size. The solution was tested up to 820 °C, which is near the upper-temperature limit for glass optical fibers. This limit could be raised significantly by using a sapphire optical fiber, which has a melting point of 2040 °C [8]. The study [40] used sapphire fibers in an environment with temperatures up to 1500 °C. However, sapphire optical fiber would also increase the price of the sensor, and therefore for solutions in environments up to 820 °C, low-cost glass optical fibers are a more cost-effective option. Although optical fiber temperature sensors are not widely used, mainly because of their high cost, they permit temperature measurement where other more common temperature measurement principles fail or cannot be used in principle or for safety reasons.

The next step in our research is mounting the sensor into an exhaust system in an experimental car and a detailed analysis of the effect on vehicle operation. Future work will also entail permanent installation on a vehicle, with monitoring conducted at various mileage intervals and recording of the effect on sensor performance under environmental influences such as poor road conditions. Additional tests must be performed to assess whether the sensor is able to reliably detect correct temperature throughout the year with changes in ambient conditions, the presence of humidity, and other factors. Rise and

drop temperature tests will also determine sensor hysteresis and reveal the stability of the direct-contact ruby-fiber coupling method.

REFERENCES

[1] T. Jeyaseelan, P. Ekambaram, J. Subramanian, and T. Shamim, "A comprehensive review on the current trends, challenges and future prospects for sustainable mobility," *Renew. Sustain. Energy Rev.*, vol. 157, Apr. 2022, Art. no. 112073.

[2] X. Xia and P. Li, "A review of the life cycle assessment of electric vehicles: Considering the influence of batteries," *Sci. Total Environ.*, vol. 814, Mar. 2022, Art. no. 152870.

[3] G. Conway, A. Joshi, F. Leach, A. García, and P. K. Senecal, "A review of current and future powertrain technologies and trends in 2020," *Transp. Eng.*, vol. 5, Sep. 2021, Art. no. 100080.

[4] Y. Nonomura, "Sensor technologies for automobiles and robots," *IEEJ Trans. Electr. Electron. Eng.*, vol. 15, no. 7, pp. 984–994, Jul. 2020.

[5] C. Zhong *et al.*, "NO_2 catalytic formation, consumption, and efflux in various types of diesel particulate filter," *Environ. Sci. Pollut. Res.*, vol. 28, no. 16, pp. 20034–20044, Apr. 2021.

[6] Y. Bin Yu and W. K. Chow, "Review on an advanced high-temperature measurement technology: The optical fiber thermometry," *J. Thermodyn.*, vol. 2009, pp. 1–11, Mar. 2009.

[7] H. Yang, W. Huang, H. Wen, and X. Y. Zhang, "Improved design of flange Mount coaxial connector with low passive intermodulation distortion," *IEEE Trans. Instrum. Meas.*, vol. 71, pp. 1–7, 2022.

[8] B. Wang, Y. Niu, X. Qin, Y. Yin, and M. Ding, "Review of high temperature measurement technology based on sapphire optical fiber," *Measurement*, vol. 184, Nov. 2021, Art. no. 109868.

[9] D. A. Resen, J. K. Hmood, and S. W. Harun, "Optical fibre sensor using frequency beating technique," *Int. J. Nanoelectron. Mater.*, vol. 13, no. 2, pp. 241–248, 2020.

[10] J. Wang, L. Wang, X. Su, R. Xiao, and H. Cheng, "Temperature, stress, refractive index and humidity multi parameter highly integrated optical fiber sensor," *Opt. Laser Technol.*, vol. 152, Aug. 2022, Art. no. 108086.

[11] S.-J. Jeon, S. Y. Park, and S. T. Kim, "Temperature compensation of fiber Bragg grating sensors in smart strand," *Sensors*, vol. 22, no. 9, p. 3282, Apr. 2022.

[12] M. Leone, "Advances in fiber optic sensors for soil moisture monitoring: A review," *Results Opt.*, vol. 7, May 2022, Art. no. 100213.

[13] E. B. Norrgard, S. P. Eckel, C. L. Holloway, and E. L. Shirley, "Quantum blackbody thermometry," *New J. Phys.*, vol. 23, no. 3, Mar. 2021, Art. no. 033037.

[14] T. J. Moore, M. R. Jones, D. R. Tree, and D. D. Allred, "An inexpensive high-temperature optical fiber thermometer," *J. Quant. Spectrosc. Radiat. Transf.*, vol. 187, pp. 358–363, Jan. 2017.

[15] S. A. Whitmore, C. I. Frischkorn, and S. J. Petersen, "*In-situ* optical measurements of solid and hybrid-propellant combustion plumes," *Aerospace*, vol. 9, no. 2, p. 57, Jan. 2022.

[16] S. Rayanasukha *et al.*, "Self-compensation for the influence of working distance and ambient temperature on thermal imaging-based temperature measurement," *IEEE Trans. Instrum. Meas.*, vol. 70, pp. 1–6, 2021.

[17] P. Franz, H. Zhu, X. Wang, R. Chia, T. Hasenberg, and H. Wang, "Tissue temperature monitoring during laser vaporization through black body radiation at wavelengths less than 1.8 μm," *Proc. SPIE*, vol. 11238, Feb. 2020, Art. no. 1123819.

[18] Y. Zhao, X. Wang, Y. Zhang, Y. Li, and X. Yao, "Optical temperature sensing of up-conversion luminescent materials: Fundamentals and progress," *J. Alloys Compounds*, vol. 817, Mar. 2020, Art. no. 152691.

[19] Q. Zhang *et al.*, "Optical thermometry of Tm^{3+}/Yb^{3+} co-doped $Ba_3Gd_2F_{12}$ up-conversion glass-ceramic with high sensitivity," *J. Solid State Chem.*, vol. 308, Apr. 2022, Art. no. 122927.

[20] L. Tang, Q. Meng, L. Bai, W. Sun, and C. Wang, "Pr^{3+}-doped $NaY(MoO_4)_2$ phosphor for optical thermometry applications," *J. Lumin.*, vol. 242, Feb. 2022, Art. no. 118570.

[21] N. Rakov, "Tm^{3+},Yb^{3+}: Y_2SiO_5 up-conversion phosphors: Exploration of temperature sensing performance by monitoring the luminescence emission," *Phys. B, Condens. Matter*, vol. 628, Mar. 2022, Art. no. 413572.

[22] K. Yang *et al.*, "An optical fiber temperature sensor based on fluorescence intensity ratio used for real-time monitoring of chemical reactions," *Ceram. Int.*, vol. 47, no. 23, pp. 33537–33543, Dec. 2021.

[23] M. Haouari, A. Maaoui, N. Saad, and A. Bulou, "Optical temperature sensing using green emissions of Er^{3+} doped fluoro-tellurite glass," *Sens. Actuators A, Phys.*, vol. 261, pp. 235–242, Jul. 2017.

[24] H. Aizawa, Y. Miyazaki, T. Katsumata, and S. Komuro, "Communication—Evaluation of fluorescent temperature sensor materials in low temperature region," *J. Electrochem. Soc.*, vol. 168, no. 1, 2021, Art. no. 017510.

[25] D. Wang and W. Pan, "Sapphire optic fiber thermometer for high temperature in tundish," *Acta Photonica Sinica*, vol. 39, no. 4, pp. 614–617, 2010.

[26] H. Aizawa, Y. Miyazaki, T. Katsumata, and S. Komuro, "Evaluation of fluorescent inorganic materials in low temperature region," in *Proc. SICE Annu. Conf.*, Aug. 2010, pp. 2660–2663.

[27] Y. Zhao, M.-Q. Chen, R.-Q. Lv, P. Wang, and X. Feng, "Small and practical optical fiber fluorescence temperature sensor," *IEEE Trans. Instrum. Meas.*, vol. 65, no. 10, pp. 2406–2411, Oct. 2016.

[28] W. Jinling and Y. Junhai, "Optic-fiber sensor based on fluorescence mechanism," in *Proc. Int. Conf. Optoelectron. Image Process.*, Nov. 2010, pp. 73–75.

[29] S. J. Mihailov, D. Grobnic, and C. W. Smelser, "High-temperature multiparameter sensor based on sapphire fiber Bragg gratings," *Opt. Lett.*, vol. 35, no. 16, pp. 2810–2812, 2010.

[30] S. Prashar, D. Engles, and S. S. Malik, "Effect of thermal expansion mismatch in grating material and host specimen on thermal sensitivity of FBG sensor," *Photonic Netw. Commun.*, vol. 34, no. 2, pp. 266–270, Oct. 2017.

[31] T. Habisreuther, T. Elsmann, A. Graf, and M. A. Schmidt, "High-temperature strain sensing using sapphire fibers with inscribed first-order Bragg gratings," *IEEE Photon. J.*, vol. 8, no. 3, pp. 1–8, Jun. 2016.

[32] V. Balakrishnan, H.-P. Phan, T. Dinh, D. Dao, and N.-T. Nguyen, "Thermal flow sensors for harsh environments," *Sensors*, vol. 17, no. 9, p. 2061, Sep. 2017.

[33] B. Rossomando, E. Meloni, G. De Falco, M. Sirignano, I. Arsie, and V. Palma, "Experimental characterization of ultrafine particle emissions from a light-duty diesel engine equipped with a standard DPF," *Proc. Combustion Inst.*, vol. 38, no. 4, pp. 5695–5702, 2021.

[34] D. J. L. Tucker *et al.*, "Thermoelectric stability of dual-wall and conventional type K and N thermocouples," *Meas. Sci. Technol.*, vol. 33, no. 7, Jul. 2022, Art. no. 075003.

[35] D. Maizak, T. Wilberforce, and A. Olabi, "$DeNO_x$ removal techniques for automotive applications—A review," *Environ. Adv.*, vol. 2, Dec. 2020, Art. no. 100021.

[36] *What is the Operating Temperature of the Engine and Why Does it Rise*. Accessed: Jan. 29, 2022. [Online]. Available: https://avtotachki.com/en/kakaya-rabochaya-temperatura-dvigatelya-i-pochemu-ona-podnimaetsya/

[37] K. Wang, S. Liu, L. Wang, J. Smulko, and H. Wen, "Novel interpolation method of multi-DFT-bins for frequency estimation of signal with parameter step change," *IEEE Trans. Instrum. Meas.*, vol. 71, pp. 1–14, 2022.

[38] W. Wen-Qing, Z. Lei, and Z. Wei-Hua, "Temperature monitoring system of electric apparatus based on optical fiber fluorescence," in *Proc. 5th Int. Conf. Intell. Syst. Design Eng. Appl.*, Jun. 2014, pp. 993–995.

[39] J. Wang *et al.*, "Fabrication of a miniaturized thin-film temperature sensor on a sapphire fiber tip," *IEEE Sensors J.*, vol. 11, no. 12, pp. 3406–3408, Jun. 2011.

[40] Y. Cui, Y. Jiang, Y. Zhang, X. Feng, J. Hu, and L. Jiang, "Sapphire optical fiber high-temperature vibration sensor," *Opt. Exp.*, vol. 30, no. 2, pp. 1056–1065, 2022.

Michal Prauzek (Member, IEEE) was born in Ostrava, Czech Republic, in 1983. He received the bachelor's degree in control and information systems, the master's degree in measurement and control systems, and the Ph.D. degree in technical cybernetics from the VSB—Technical University of Ostrava (VSB-TUO), Ostrava, in 2006, 2008, and 2011, respectively.

He has worked as a Research Post-Doctoral Fellow with the University of Alberta, Edmonton, AB, Canada, from 2013 to 2014. He has been working with the Department of Cybernetics and Biomedical Engineering, VSB-TUO, since 2010, where he is currently an Associate Professor. He has authored more than 80 articles and conference papers and has eight registered inventions. His research topics include embedded systems, data and signal analysis, control design, and machine learning.

Dr. Prauzek is an IEEE Member active in the Systems, Man and Cybernetics Society and the Engineering in Medicine and Biology Society.

Radim Hercik was born in Ostrava, Czech Republic, in 1987. He received the bachelor's degree in control and information systems, the master's degree in measurement and control engineering, and the Ph.D. degree in technical cybernetics, from VSB—Technical University of Ostrava, Ostrava, in 2009, 2011, and 2014, respectively.

His professional career includes the position as a Developer of ultrasonic automotive sensors at Continental Automotive Czech Republic s.r.o., Jicin, Czech Republic, until 2020. He has been working with the Department of Cybernetics and Biomedical Engineering, VSB—Technical University of Ostrava, since 2020, where he is currently an Assistant Professor. He is the author of more than 20 articles and conference papers and has six registered inventions. His research topics include embedded systems, automation, industrial robotics, and mobile robotics.

Jaromir Konecny was born in Frydek-Mistek, Czech Republic, in 1986. He received the bachelor's degree in control and information systems, the master's degree in measurement and control engineering, and the Ph.D. degree in technical cybernetics, from VSB—Technical University of Ostrava, Ostrava, Czech Republic, in 2008, 2010, and 2014, respectively.

He has been working with the Department of Cybernetics and Biomedical Engineering, VSB—Technical University of Ostrava, since 2012, where he is currently an Assistant Professor. He is the author of more than 40 articles and conference papers and has four registered inventions. His research topics include embedded systems, electronics, environmental monitoring systems, and localization systems in robotics.

Martin Mikolajek was born in Opava, Czech Republic, in 1988. He received the bachelor's degree in measurement and control engineering, the master's degree in measurement and control engineering, and the Ph.D. degree in technical cybernetics from the VSB—Technical University of Ostrava (VSB-TUO), Ostrava, Czech Republic, in 2010, 2013, and 2021, respectively.

Since 2016, he has been working as a Researcher with the Department of Cybernetics and Biomedical Engineering, VSB-TUO, where he is currently an Assistant Professor. His professional career includes programming, industrial automation systems and simulation of control and visualization systems, and design of electrical circuits. His pedagogical practice relates to industrial automation systems. He has collaborated on several articles which investigate measurement and industrial automation.

Martin Stankus was born in Olomouc, Czechoslovakia, in 1983. He received the master's degree in computer science and the Ph.D. degree in technical cybernetics from the VSB—Technical University of Ostrava (VSB-TUO), Ostrava, Czech Republic, in 2009 and 2017, respectively.

He is currently an Assistant Professor with VSB-TUO. His domain of expertise includes microprocessor technology, embedded system design, and digital technology in general. He has cooperated on multiple articles and conference papers directed at embedded system design. His research topics include microcontrollers and digital systems, electronics, wireless communications systems, the IoT technologies, and embedded technology.

Jiri Koziorek is currently a Full Professor in cybernetics with the VSB—Technical University of Ostrava (VSB-TUO), Ostrava, Czech Republic. He has been working with the Department of Cybernetics and Biomedical Engineering, VSB-TUO, since 1998, where he has been the Head of the Department since 2009. His research interests cover industrial automation, control system design, industrial communications, digitization of industry, and sensors. His pedagogical practice relates to his research areas. He is a coordinator of several national and international research projects, typically in cooperation with industrial partners. He is the author/coauthor of more than 100 scientific publications.

Radek Martinek (Senior Member, IEEE) is currently a Full Professor of cybernetics with the Faculty of Electrical Engineering and Computer Science, VSB—Technical University of Ostrava, Ostrava, Czech Republic. He has been serving as the Vice-Dean for science and research and the Deputy Head of the Department of Cybernetics and Biomedical Engineering. His research is mainly focused on hybrid and bio-inspired methods for advanced signal processing. His research activities closely correlate with his pedagogical practice. The main priority of his research activities is the high applicability of results and deployment of novel experimental algorithms in the field of cybernetics and biomedical engineering. He is the author of more than 300 publications with more than 2000 citations and an H-index of 21. He also holds ten Czech national patents and is the leader and a co-leader of dozens of projects with budgets of millions of euros.